Boundary-Layer Meteorol (2009) 130:327–345
DOI 10.1007/s10546-009-9356-8

ORIGINAL PAPER

Dissimilarity of Scalar Transport in the Convective Boundary Layer in Inhomogeneous Landscapes

Jianping Huang · Xuhui Lee · Edward G. Patton

Received: 3 June 2008 / Accepted: 26 January 2009 / Published online: 8 February 2009

Abstract A land-surface model (LSM) is coupled with a large-eddy simulation (LES) model to investigate the vegetation-atmosphere exchange of heat, water vapour, and carbon dioxide (CO_2) in heterogeneous landscapes. The dissimilarity of scalar transport in the lower convective boundary layer is quantified in several ways: eddy diffusivity, spatial structure of the scalar fields, and spatial and temporal variations in the surface fluxes of these scalars. The results show that eddy diffusivities differ among the three scalars, by up to 10–12%, in the surface layer; the difference is partly attributed to the influence of top-down diffusion. The turbulence-organized structures of CO_2 bear more resemblance to those of water vapour than those of the potential temperature. The surface fluxes when coupled with the flow aloft show large spatial variations even with perfectly homogeneous surface conditions and constant solar radiation forcing across the horizontal simulation domain. In general, the surface sensible heat flux shows the greatest spatial and temporal variations, and the CO_2 flux the least. Furthermore, our results show that the one-dimensional land-surface model scheme underestimates the surface heat flux by 3–8% and overestimates the water vapour and CO_2 fluxes by 2–8% and 1–9%, respectively, as compared to the flux simulated with the coupled LES-LSM.

Keywords Carbon dioxide fluxes · Land-surface coupling · Land-surface scheme · Scalar transport · Surface heterogeneity

1 Introduction

Understanding vegetation-atmosphere interactions is essential to climate modelling and ecological sciences since the surface fluxes provide lower boundary conditions for numerical

J. Huang (✉) · X. Lee
School of Forestry and Environmental Studies, Yale University, New Haven, CT, USA
e-mail: jianping.huang@yale.edu

E. G. Patton
National Center for Atmospheric Research, Boulder, CO, USA

models. The theoretical framework for quantifying these boundary conditions is the Monin-Obukhov (MO) similarity theory, which states that the transport of heat, water vapour, CO_2 and other scalars can be described by the same set of universal non-dimensional functions. When surface heterogeneities are present, or in situations where the vertical source distributions of these constituents differ, the similarity assumption is often violated (e.g., Denmead and Bradley 1985; McNaughton and Laubach 1998; Lee et al. 2004).

The dissimilarity of scalar transport manifests itself in a number of quantifiable ways. Most commonly, eddy diffusivity is assumed to be equal for all passive scalars. For example, in the modified Bowen-ratio applications, the eddy diffusivity of heat is used to estimate the fluxes of water vapour, CO_2, and other trace gases. However, the assumption is often not satisfied in the real world. One piece of evidence of the dissimilarity is the small correlation coefficients between the fluctuations in temperature, water vapour and CO_2 concentration (Denmead and Bradley 1985). McNaughton and Laubach (1998) argued that the small correlation coefficient is a necessary but not sufficient condition for the dissimilarity, and suggested that incomplete adjustment of the turbulent transport processes, non-stationarity, and the external wind are responsible for the non-similarity of the eddy diffusivities for sensible heat (K_H) and water vapour (K_W) near the bottom of an internal boundary layer formed downwind of a dry-to-wet transition. McNaughton and Laubach (1998) and Lee et al. (2004) further linked the inequality of eddy diffusivities between heat and water vapour to diffusion from multiple sources. Lee et al. (2004) presented a theoretical analysis of dual-source diffusion to predict that entrainment at the top of the boundary layer could cause an inequality of K_H and K_W in the surface layer. This prediction has not been verified by experiments or model simulations.

The dissimilarity of transport can be also understood by examining the temporal and spatial variations of the scalar fields. In a large-eddy simulation (LES) study, Jonker et al. (1999) showed that the peak wavelength of the vertical velocity and potential temperature fluctuations in the middle of the convective boundary layer (CBL) is much shorter than that of water vapour, and attributed the difference to the influence of entrainment. The entrainment also influences the coherent structures. For example, Huang et al. (2008) demonstrated that the flux imbalance of heat and a bottom-up tracer is tightly associated with turbulence-organized structures (TOSs), whereas such relationships are weak to non-existent for top-down diffusion. They also found that the vertical flux of the bottom-up tracer at the mixed-layer top is about 4.5% of the surface flux. The TOS is a ubiquitous feature of the convective boundary layer and efficient in transporting heat, water vapour and other scalars in the CBL. Kanda et al. (2004b) found that TOSs partially accounted for the spatial variations in the momentum flux in their LES model domain. Gao et al. (1989) observed ramp patterns of temperature and humidity within and above a forest canopy and used them to identify coherent structures under both unstable and near-neutral conditions. Paw et al. (1992) and Su et al. (1996) noted that the temporal variation in CO_2 concentration in the intercellular space and at the leaf surface is different from variations in air temperature and water vapour, and showed that ramp-like structures of the scalar time series are associated with TOSs in turbulent flow.

The existence of TOSs raises questions about the extent to which land-surface models (LSM) misrepresent the true land-atmosphere interactions. It is known that TOSs exist even when the surface boundary conditions are uniform across the horizontal domain. Therefore, from the land-surface modelling perspective, the flow in the atmospheric boundary layer (ABL) is essentially heterogeneous because the factors influencing land-atmosphere interactions, such as wind speed and vapour pressure deficit, will vary across the TOSs. Furthermore, in the presence of surface heterogeneity, mesoscale motions occur (e.g., Avissar and Schmidt

1998). In a typical LSM application in numerical weather prediction (NWP) and climate models, the grid size is usually larger than the horizontal dimension of the TOSs or the mesoscale motions. The LSM is driven by single-valued surface parameters assigned to the model domain, such as soil moisture, and by the domain-averaging meteorological inputs, such as wind speed, temperature, and air humidity. In other words, LSMs are one-dimensional (1D) parameterizations by design. In the 1D framework, the computed fluxes of sensible heat, water vapour, and CO_2 do not include the effects associated with the surface and ABL flow heterogeneity.

Aggregated models have been proposed as a remedy to handle the problem of parameter nonlinearity associated with surface heterogeneity (Doran et al. 1998). These models are driven by surface conditions at individual "patches" of the landscape within a grid cell, each having its own soil moisture and vegetation type, and the surface fluxes are scaled up to the whole grid by a simple algebraic averaging scheme. This method accounts for the influences resulting from the parameter nonlinearity within the grid but does not consider the impact associated with the ABL flow heterogeneity. The effects of flow heterogeneity are likely to be different for heat, water vapour and carbon dioxide.

Several LES studies have shown evidence that dissimilarity in transport between heat and water vapour can arise from land-surface heterogeneity. Hadfield et al. (1991, 1992) observed that surface heterogeneity induces organized circulations whose intensity increases with increasing wavelength and decreases with increasing wind speeds. Shen and Leclerc (1995) and Avissar and Schmidt (1998) further examined the scale at which the surface heterogeneity begins to significantly influence the coherent structures in the CBL. Recently, Patton et al. (2005) and Courault et al. (2007) dynamically coupled a LSM with LES, and in the coupled mode, the LES was driven by the time-varying surface fluxes predicted by the LSM instead of prescribed values. Patton et al. (2005) showed that the impact of surface heterogeneity depends on the scale of heterogeneity (λ). The strongest organized motions occur when the ratio λ/z_i (z_i is boundary-layer height) has a value ranging from 4 to 9. Courault et al. (2007) investigated the impact of stripe-like and chessboard-like surface heterogeneities at a fine scale (1 km) on the flow structure in the CBL, and showed that the CBL responds to the spatial configurations of surface heterogeneity. In these studies, attention was given to the impact of surface heterogeneity on the scalar fields and flow structures in the CBL. However, the coupled LES-LSM system also provides a tool for investigating how the surface fluxes respond to the spatially varying flow and scalar fields. Since the biophysical processes controlling the exchanges of sensible heat, water vapour and carbon dioxide are quite different, we expect their fluxes to behave differently when coupled with turbulent flow in the CBL.

In this study, we have reworked the LES-LSM coupling to include CO_2 exchange. In the earlier work, Patton et al. (2005) used the National Centers for Environmental Prediction/Oregon State University/Air Force/Office of Hydrogology (NOAH) LSM (Ek et al. 2003). We have replaced NOAH with an $A_g - g_{c,w}$ approach, where A_g is the gross assimilation rate and $g_{c,w}$ is the canopy conductance to water vapour flow (Ronda et al. 2001). As compared to the traditional Jarvis-Stewart method (Jarvis 1976) embedded in NOAH, the $A_g - g_{c,w}$ approach is based on plant physiology theory and is better suited for studying the dynamic feedback between canopy conductance, CO_2 flux and surface energy balance. Our goal is to quantify how surface and flow heterogeneities affect the exchange of heat, water vapour and CO_2 in the lower ABL. The coupled LES-LSM is an ideal tool to achieve this goal because, (a) it has the capability of specifying surface heterogeneity in the whole domain, (b) it explicitly resolves the flow heterogeneity, and (c) it gives a prediction of the dynamic feedbacks between the surface fluxes, the ABL flow, and entrainment. Most relevant LES studies have

been interested in how surface conditions influence the dynamics of the ABL flow. Here our attention is on how the flow dynamics modulate the surface fluxes. Our specific objectives are, (a) to investigate the inequality of the eddy diffusivities for heat, water vapour and CO_2 in the surface layer, (b) to determine the magnitude of and mechanisms responsible for the spatial variations of the surface heat, water vapour and CO_2 fluxes with uniform soil moisture and vegetation conditions, and (c) to quantify the extent to which the 1D LSM schemes in NWP and climate models misrepresent the true vegetation-atmosphere interactions.

2 Coupling of LES with LSM

2.1 LES Model

The NCAR LES model has been described by Moeng (1984); Sullivan et al. (1996) and Patton et al. (2005). In this study, the LES is coupled with a LSM to reproduce the dynamic vegetation-atmosphere interactions and to provide a benchmark to judge the representativeness of 1D flow parameterization schemes in NWP and climate models.

2.2 Land-Surface Model

The LSM provides the time-dependent surface fluxes including heat, water vapour, and CO_2 to drive the LES model. As with other LSMs, the surface skin temperature (T_s) is solved from the surface energy balance equation

$$(1-a)K^{\downarrow} + \varepsilon L^{\downarrow} - \varepsilon\sigma T_s^4 = H + LE + S, \tag{1}$$

where $K^{\downarrow}$ and $L^{\downarrow}$ are the incoming solar and longwave radiation fluxes at the surface, respectively, a is albedo, ε is surface emissivity, σ is the Stephan-Boltzman constant, H is the surface sensible heat flux, LE is the surface latent heat flux, and S is the heat storage term between the surface and the soil reference level.

The sensible (H) and latent (LE) heat fluxes depend on surface skin temperature and local atmospheric conditions at the reference level (i.e., the first level of the LES model)

$$H = \rho_a c_p g_a (T_s - T_a), \tag{2a}$$

$$LE = \rho_a L g_a \left(\frac{q^*(T_s) - q_a}{1 + g_a/g_{c,w}} \right), \tag{2b}$$

where ρ_a is air density, c_p specific heat at constant pressure, T_a and q_a are air temperature and specific humidity at the reference level, respectively, g_a is the aerodynamic conductance calculated with the MO similarity theory (Beljaars and Holtslag 1991), and $g_{c,w}$ is canopy conductance to water vapour flow, which is 1.6 times the canopy conductance to CO_2, $g_{c,c}$.

The $A_g - g_{c,w}$ approach calculates the net flux of CO_2 into the canopy as follows:

$$A_n = A_g - R_d = A_g - 0.11A_m, \tag{3}$$

where R_d is the dark respiration rate, A_m is the maximal primary productivity given by

$$A_m = A_{m,\max}\{1 - e^{-[g_m(C_i - \Gamma)/A_{m,\max}]}\} f_5, \tag{4}$$

where $A_{m,\max}$ is the maximal primary productivity under high light conditions and high CO_2 concentration, g_m is the mesophyll conductance, Γ is the CO_2 compensation point, and f_5 is a function of soil moisture with values ranging from 0 (the driest case) to 1 (the wettest case).

The gross primary productivity, A_g, is proportional to $A_m + R_d$, with the proportionality coefficient dependent on light use efficiency and photosynthetically active radiation (PAR) absorption by the canopy.

The surface conductance $g_{c,w}$ (or $g_{c,c}$) is a key parameter used to calculate *H, LE*, and A_n (Ronda et al. 2001). The canopy conductance $g_{c,c}$ shows a highly nonlinear dependence on parameters such as PAR, the internal CO_2 concentration, the CO_2 concentration at the reference height, leaf area index, and soil moisture. More details can be found in Ronda et al. (2001).

3 LES-LSM Configurations

Soil moisture (via parameter f_5) is an important factor in controlling canopy conductance, and eventually determining T_s, the partitioning of available energy into *H* and *LE*, and the net exchange of CO_2. As illustrated in Fig. 1, T_s and surface fluxes show strong dependence on the soil moisture parameter f_5. While both T_s and *H* decrease with increasing soil moisture (f_5), LE and A_n follow an opposite relationship with f_5. In the following, we use f_5 as a proxy to represent the surface moisture heterogeneity.

In this study, five sets of coupled LES-LSM simulations corresponding to different spatial patterns of soil moisture were conducted over a domain of size 9.6 km × 6.0 km × 1.92 km, and grid-spacing of 50 m × 50 m × 10 m in the *x, y*, and *z* directions, respectively. Our simulations include two homogeneous (labelled as A and B, representing dry and wet cases,

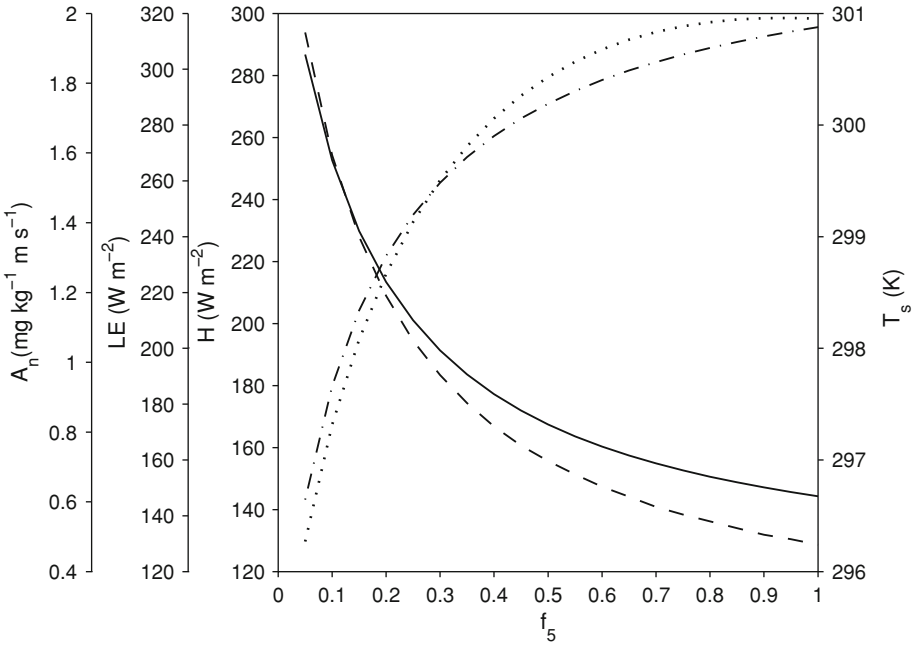

Fig. 1 Sensitivity of T_s, H, LE, and A_n to f_5, a parameter representing soil moisture: solid line, T_s (surface skin temperature, K); dash line, H (sensible heat flux, $W\,m^{-2}$); dashed dotted line, LE (latent heat flux, $W\,m^{-2}$); dotted line, A_n (CO_2 flux, $mg\,kg^{-1}\,m\,s^{-1}$)

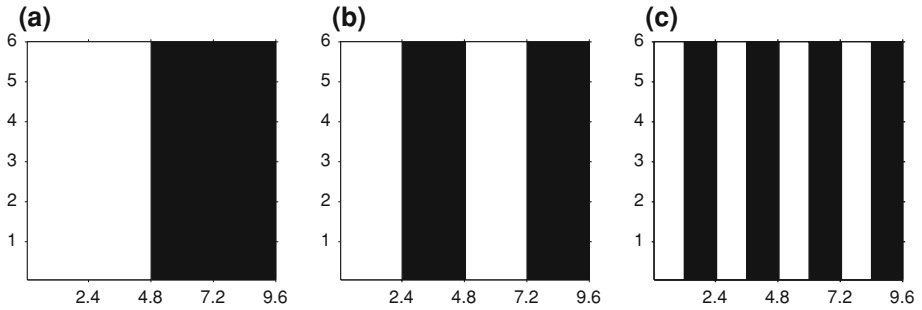

Fig. 2 Spatial patterns of soil moisture: **a** $a = 1/2$, **b** $a = 1/4$, and **c** $a = 1/8$ (*white*: dry stripe with $f_5 = 0.1$; *black*: wet stripe with $f_5 = 0.3$). The full domain size is 9.6 km × 6.0 km

Table 1 Details of LES simulations

Cases	u_g (m s^{-1})	Striped pattern (a)	f_5
A	0, 2, 4, 6	1	0.1
B	0, 2, 4, 6	1	0.3
C	0, 2, 4, 6	1/2	0.1/0.3
D	0, 2, 4, 6	1/4	0.1/0.3
E	0, 2, 4, 6	1/8	0.1/0.3

respectively) and three surface heterogeneous cases (labelled as C, D, and E for the stripe cases with $a = 1/2$, 1/4, and 1/8, respectively, where a denotes the ratio of the stripe width to the whole domain size). The surface heterogeneities follow a step-function variation between dry ($f_5 = 0.1$) and wet ($f_5 = 0.3$) stripes along the x-direction (Fig. 2). Each surface pattern was performed with geostrophic winds of 0, 2, 4, and 6 m s^{-1}, giving a total of twenty simulations (Table 1).

All LES simulations were initiated with profiles of potential temperature (θ), specific humidity (q), and CO_2 concentration (C) that were uniform in the horizontal directions over the domain, as shown in Fig. 3. The initial θ profile was set to a constant within the mixed layer, with an initial boundary-layer depth set to 960 m in all simulations, a vertical gradient of 0.075 K m^{-1} in the interfacial layer, and a vertical gradient of 0.003 K m^{-1} in the free atmosphere. The initial q profile was set at a constant within the mixed layer, a decreasing rate of 0.175 g kg^{-1} m^{-1} in the interfacial layer, and a constant value above. The initial C profile consisted of a constant value within the mixed layer, a strong gradient of 0.75 mg kg^{-1} m^{-1} across the interfacial layer and a constant value above the interfacial layer. The external forcing is the incoming solar radiation, which is constant in time and uniform throughout the domain (700 W m^{-2}). The incoming longwave radiation $L^{\downarrow}$ is parameterized with an Idso-type scheme (Idso 1981).

As in our previous studies (Patton et al. 2005; Huang et al. 2008), the post-processing analyses of the LES-LSM data were performed after the turbulent kinetic energy had reached a quasi-steady level, usually after about 120 min of integration time. The timesteps during each simulation were dynamically determined based on the Courant-Friedrichs-Lewy (CFL) number.

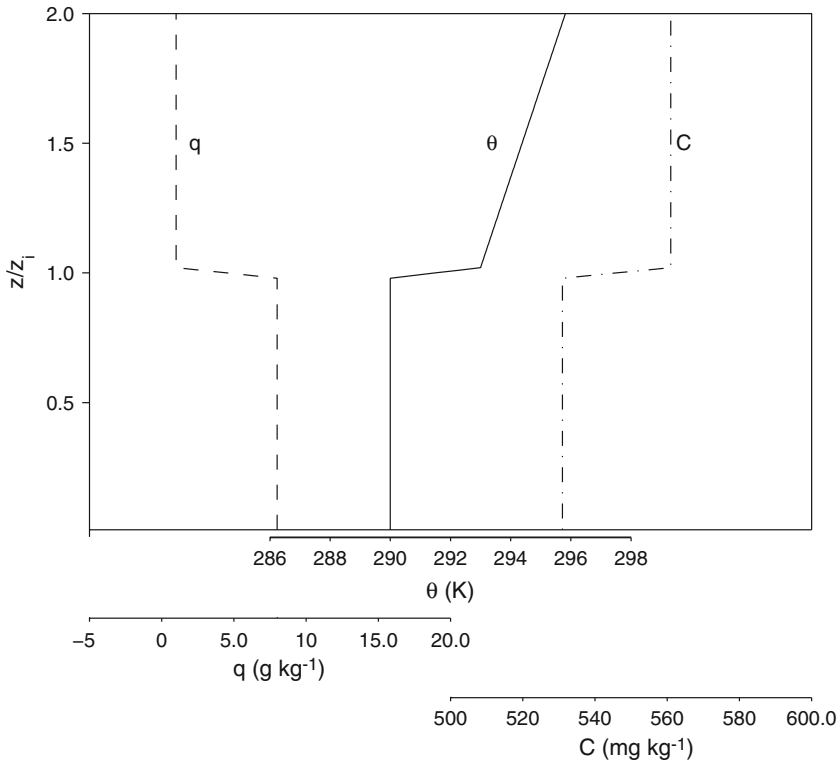

Fig. 3 Initial profiles of potential temperature (θ, *solid line*), specific humidity (q, *dashed line*), and CO_2 mixing ratios (C, *dash-dotted line*)

4 Model Results and Analyses

4.1 Total Flux Profiles

Figure 4 shows hourly-averaged vertical profiles of normalized total fluxes, defined as the sum of the resolved and subgrid-scale (SGS) fluxes, of heat ($\overline{\rho_a c_p \langle w''\theta''\rangle}/H$), virtual potential temperature ($\overline{\langle w''\theta_v''\rangle}/(w_*\theta_{v*})$), water vapour ($\overline{\rho_a \langle w''q''\rangle}/E$), and CO_2 ($\overline{\langle w''c''\rangle}/A_n$) for the homogeneous wet case and three cases of the striped patterns under free convective conditions ($u_g = 0$). In Fig. 4, the convective velocity is defined as $w_* = \left(\frac{gz_i}{\rho_a}\left(\frac{H}{\theta_0 c_p} + 0.61E\right)\right)^{\frac{1}{3}}$, where g is the gravitational acceleration, z_i is the mixing-layer height, θ_0 is a reference potential temperature, E is surface evaporation, the virtual potential temperature is given by $\theta_v = \theta(1 + 0.61q)$, and the virtual temperature scale is defined as $\theta_{v*} = (H/c_p + 0.61\theta_0 E)/(\rho_a w_*)$.

The flux profiles are linear with z/z_i and are shown to emphasize that each of the three scalars being considered here are responding to different entrainment/surface flux ratios. The entrainment-to-surface flux ratio for buoyancy (virtual potential temperature, Fig. 4b) varies from -0.14 to -0.17 which is very close to Deardorff's (1979) theoretical value of -0.2. For heat, the magnitude of the entrainment flux is about 30% that of the surface (and of opposite sign); while for moisture, entrainment is about three times larger than the surface flux (and of

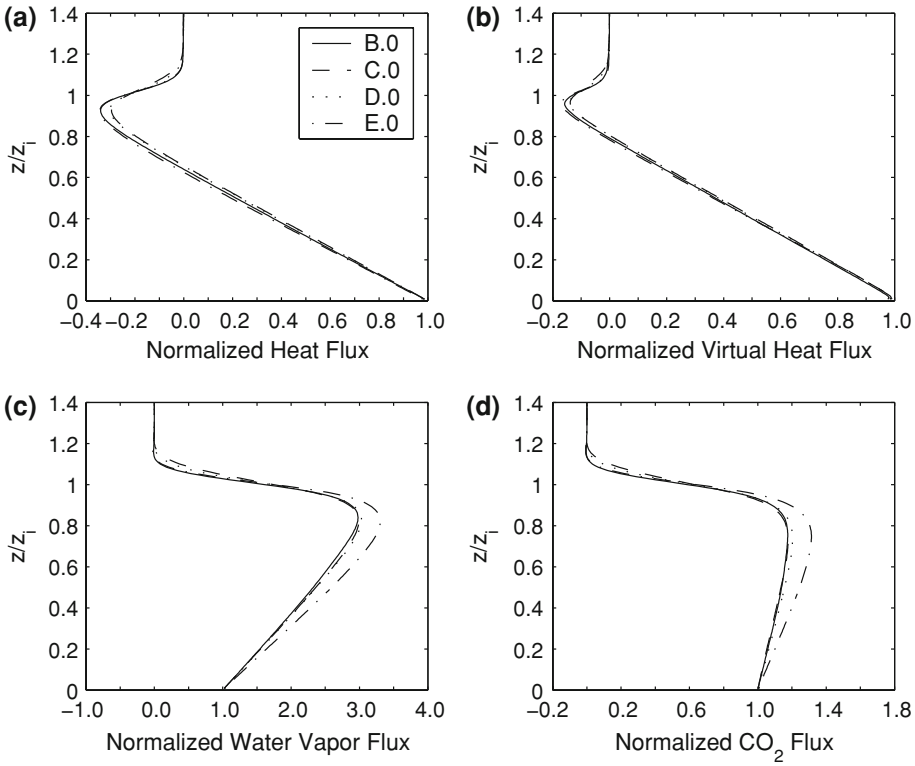

Fig. 4 Vertical profiles of normalized fluxes of **a** heat ($\overline{\rho c_p \langle w''\theta'' \rangle}/H$), **b** virtual potential temperature ($\overline{\langle w''\theta_v'' \rangle}/(w_* \theta_{v*})$), **c** water vapour ($\overline{\rho \langle w''q'' \rangle}/E$), and **d** CO_2 ($\overline{\langle w''c'' \rangle}/A_n$) for homogeneous case (B) and stripe cases of $a = 1/2$ (C), $a = 1/4$ (D), $a = 1/8$ (E), all under $u_g = 0$

similar sign). In contrast, the entrainment and surface fluxes of CO_2 are of similar magnitude, where both are directed downward. Consistent with the results of Patton et al. (2005), our simulations show that surface heterogeneity has a negligible impact on the total normalized virtual heat flux profiles compared to a homogeneous surface, and has a minor impact on the water vapour and CO_2 flux profiles.

4.2 Eddy Diffusivity

Eddy diffusivity is a useful parameter for describing the efficiency of scalar transport in the ABL. In this section, we revisit the issue of the inequality of eddy diffusivities for sensible heat (K_h), water vapour (K_q), and CO_2 (K_c), and restrict the analysis to the surface layer ($z/z_i < 0.05$, where z_i varies in the range of 1105–1157 m during the analyzed period). The flux-gradient relationship is expressed as

$$\overline{\langle w''\theta'' \rangle} = -K_h \frac{\partial \overline{\langle \theta \rangle}}{\partial z}, \tag{5a}$$

$$\overline{\langle w''q'' \rangle} = -K_q \frac{\partial \overline{\langle q \rangle}}{\partial z}, \tag{5b}$$

$$\overline{\langle w''c''\rangle} = -K_c \frac{\partial \overline{\langle c\rangle}}{\partial z}, \tag{5c}$$

where $\overline{\langle w''\theta''\rangle}$, $\overline{\langle w''q''\rangle}$, and $\overline{\langle w''c''\rangle}$ represent domain-averaged sensible heat, water vapour, and CO_2 fluxes including the SGS contribution, respectively, $\partial\overline{\langle\theta\rangle}/\partial z$, $\partial\overline{\langle q\rangle}/\partial z$, and $\partial\overline{\langle c\rangle}/\partial z$ denote the vertical gradients of the domain-averaging potential temperature, water vapour, and CO_2, respectively, and the overbar denotes time averaging usually over an interval of 1 h. Eqs. 5a–c are used to determine K_h, K_q, and K_c from the LES fields of these scalars and their vertical fluxes. The SGS contribution increases from 20%, 17% and 19% at $u_g = 0$ to 33%, 31%, and 32% at $u_g = 6\,\mathrm{m\,s^{-1}}$ for heat, water vapour and CO_2 in case A, respectively, indicating an increased reliance on the SGS model at higher wind speeds within the lower part of the ABL (15–45 m above ground level in this study). In comparison, the SGS contribution is not sensitive to surface heterogeneity. To account for the SGS effect, we used a new SGS eddy-viscosity model (Sullivan et al. 1994) in the LES simulations to examine the relationship between the LES and the Monin-Obukhov similarity functions.

Our LES simulations show that in the surface layer K_h is smaller than K_q, and K_c lies between K_h and K_q (Fig. 5). The mean value of K_q/K_h is 1.12 and K_c/K_h 1.10 in the layer 15–45 m above the ground level. Our K_q/K_h ratio is slightly smaller than the observed value of 1.26 for unstable conditions reported by Lee et al. (2004). The eddy diffusivities simulated with heterogeneous surface forcing lie between the values for the dry and wet homogeneous cases. The difference between the three heterogeneous cases ($a = 1/2$, 1/4 and 1/8) is indistinguishable.

Two factors responsible for the inequality of the eddy diffusivities are local advection induced by the surface moisture heterogeneity and the influence of top-down diffusion

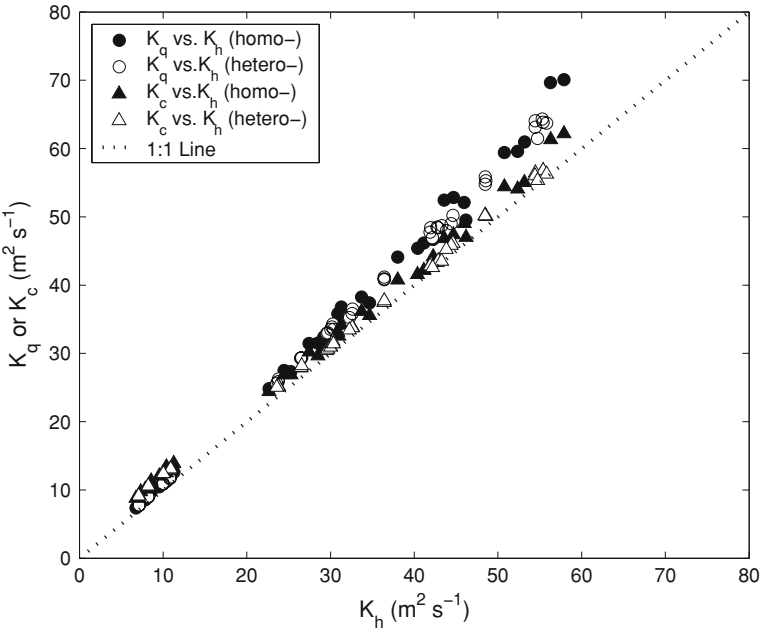

Fig. 5 Comparison of eddy diffusivities of water vapour (K_q) and CO_2 (K_c) with that of heat (K_h) for LES grid level 2 to 5 for all the five cases shown in Table 1

associated with entrainment at the top of the ABL. Our simulations suggest that the second factor is more important than the first.

The eddy diffusivities are related to the MO similarity functions ϕ_h, ϕ_q, and ϕ_c for the three scalars, as

$$\phi_h = \frac{\kappa z u_*}{K_h}, \tag{6a}$$

$$\phi_q = \frac{\kappa z u_*}{K_q}, \tag{6b}$$

$$\phi_c = \frac{\kappa z u_*}{K_c}, \tag{6c}$$

where κ is the von Kármán constant, and u_* is the friction velocity computed as

$$u_* = ((-\overline{\langle u''w''\rangle})^2 + (-\overline{\langle v''w''\rangle})^2)^{0.25}, \tag{7}$$

where $\overline{\langle u''w''\rangle}$ and $\overline{\langle v''w''\rangle}$ are the longitudinal and lateral components of the temporally-averaged spatial covariance, respectively, and z is height. These similarity functions are plotted against $-z/L$ in Fig. 6, where L is the Obukhov length. The data points represent the LES simulations at levels 2, 3, 4, and 5 corresponding to heights 15, 25, 35, and 45 m above the ground and include both homogeneous (simulations A and B) and heterogeneous surface conditions (simulations C, D and E, Table 1). Each point shown in Fig. 6 corresponds to a value at one level. These data are compared with the standard function for heat (Dyer 1974)

$$\phi_h = \begin{cases} (1 - 16z/L)^{-0.5}, & -5 < z/L < 0 \\ 1 + 5z/L, & 1 > z/L \geq 0 \end{cases} \tag{8}$$

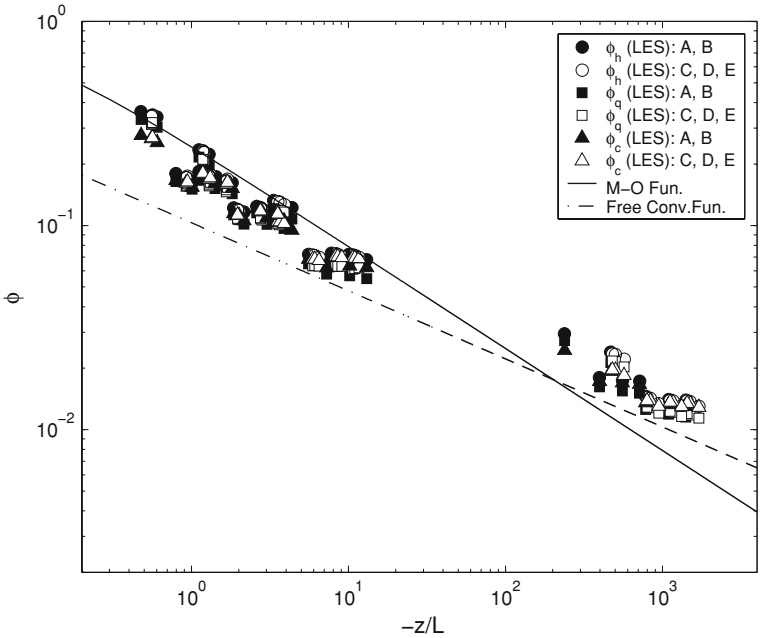

Fig. 6 Comparison among the LES predictions, the MO similarity function and the free convection function

and the free convective limit given by Garratt (1992)

$$\phi_h = 0.7\kappa^{4/3}(-z/L)^{-1/3}. \tag{9}$$

We note that Eq. 8 is also used in the LSM for determining the aerodynamic conductance in Eqs. 2a, 2b.

Consistent with previous LES analyses of scalar stability functions (e.g., Sullivan et al. 1994), the LES overpredicts standard stability functions when $-z/L > 5$ (or underpredicts when $-z/L < 5$). Nevertheless, the variation in the flux-gradient relationships across scalar type is noteworthy; for the same stability class (z/L), we find that $\phi_h < \phi_c < \phi_q$. This dissimilarity implies that heat, moisture and carbon dioxide are transported unequally and that their eddy diffusivities differ. The free convective limit (Eq. 9) is rarely confirmed experimentally because of the difficulty in attaining the condition of free convection. Our LES results suggest that this limit is not achieved with the data points for $z/L > -20$ (Fig. 6).

4.3 Spatial Variations in Scalar Fields

It is well known that TOSs exist in the vertical velocity and temperature fields (e.g., Kanda et al. 2004a; Huang et al. 2008). Here we wish to explore whether similar structures also exist in the water vapour and CO_2 fields and how the surface heterogeneity influences TOSs and the scalar transport. Under free convective conditions, the structures similar to those in the temperature field appear in the water vapour and CO_2 fields with homogeneous surface conditions (simulations A and B; data not shown). However, the TOSs of the three scalars are modified dramatically by the surface moisture heterogeneity. As an example, Fig. 7 shows the horizontal cross-sections of the hourly-averaged potential temperature, specific humidity, and CO_2 concentration at $z = 35$ m above the ground for the striped pattern $a = 1/2$ with $u_g = 0$ and $4\,\mathrm{m\,s^{-1}}$. The impact of the surface heterogeneity differs among the three scalars. At $u_g = 0$ (free convection), while the water vapour TOSs are clearly discernable across the whole domain, the temperature TOSs are more fragmented at smaller scales particularly over the wet strip. The CO_2 TOSs bear much resemblance to those of water vapour but with an opposite phase to water vapour because CO_2 is more depleted over the wet stripe due to more vigorous photosynthetic uptake and increased transpiration.

Another striking feature is that the three scalars display roll-like structures aligned along the wind directions at $u_g > 0$. In the case of temperature and water vapour, the roll structures are strong enough to almost mask the influence of the step change in soil moisture. Roll structures, also reported by Mahrt (1998) and Steinfeld et al. (2007), affect the tower flux measurement and energy imbalance measured with eddy-covariance instruments.

4.4 Spatial and Temporal Variations in Surface Fluxes

The surface fluxes, the main factor driving the development of the CBL, are regulated dynamically through the coupled surface-atmosphere system. Most previous modelling studies assume that surface fluxes at individual grid points are invariant with time. Here we use the fully coupled LES-LSM model to resolve the response of surface fluxes to soil moisture availability and feedbacks from the ABL flow and other meteorological fields.

Figure 8 depicts horizontal distributions of hourly-averaged surface sensible heat, latent heat, and CO_2 fluxes under homogenous soil moisture forcing ($f_5 = 0.3$). Fluctuations of the surface fluxes are found throughout the domain, even though the initial conditions are uniform horizontally and the incident shortwave radiation is constant in time and space

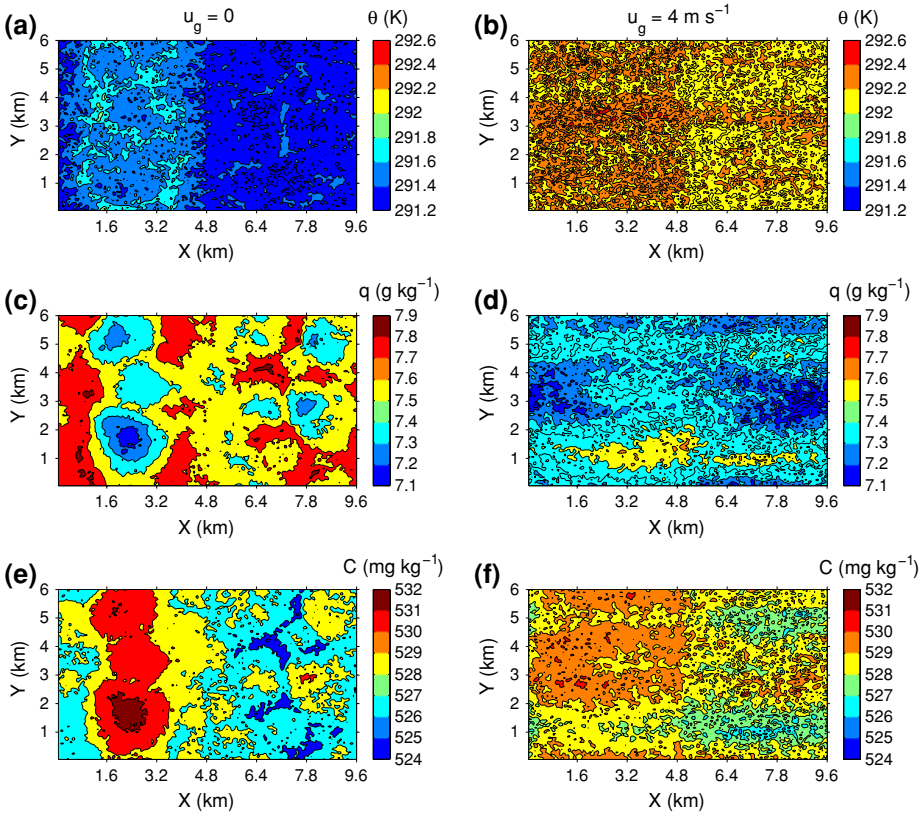

Fig. 7 Hourly-averaged fields of potential temperature (θ, K, *panels a* and *b*), water vapour (q, g kg^{-1}, *panels c* and *d*), carbon dioxide concentrations (C, mg kg^{-1}, *panels e* and *f*) for the stripe case C ($a = 1/2$) at the height z=35 m under free ($u_g = 0$, *left side*) and forced convection ($u_g = 4\,\mathrm{m\,s^{-1}}$, *right side*) conditions

($K^{\downarrow}$ in Eq. 1). These fluctuations occur at much finer spatial scales than those in the three scalar fields. Interestingly, the CO_2 flux displays discernable TOSs under free convection but the heat flux does not. A spectral analysis reveals that the dominant wavelength of the fluctuations differs among the three fluxes in the streamwise direction ($0.23z_i$ for sensible heat flux versus $0.46z_i$ for latent heat and CO_2 fluxes). In the cross-wind direction, the fluctuations in the fluxes tend to be dominated by motions at scales greater than $0.86z_i$ (Fig. 9). The cospectra differ from the "classic" spectrum of a boundary-layer turbulence variable, the latter showing a dominant wavelength at the scale of the boundary-layer height (Jonker et al. 1999). The increase in mechanical turbulence due to increasing u_g has the effect of damping the spatial variations in the surface fluxes. The sensible heat flux has the highest spatial variability and the CO_2 flux the lowest. The coefficient of variation (CV) for the simulations shown in Fig. 10 is 0.010, 0.006, and 0.0027 for sensible heat, latent heat and CO_2 flux, respectively, under free convection ($u_g = 0$) and 0.007, 0.004, and 0.0017 under forced convection ($u_g = 4\,\mathrm{m\,s^{-1}}$).

To understand the mechanism underlying the spatial variations, in Table 2 we present the correlation coefficients (C_r) between the simulated surface fluxes (H, LE, A_n) and temperature (T_s) and the scalar wind speed (U), air temperature (T_a), specific humidity (q), and CO_2

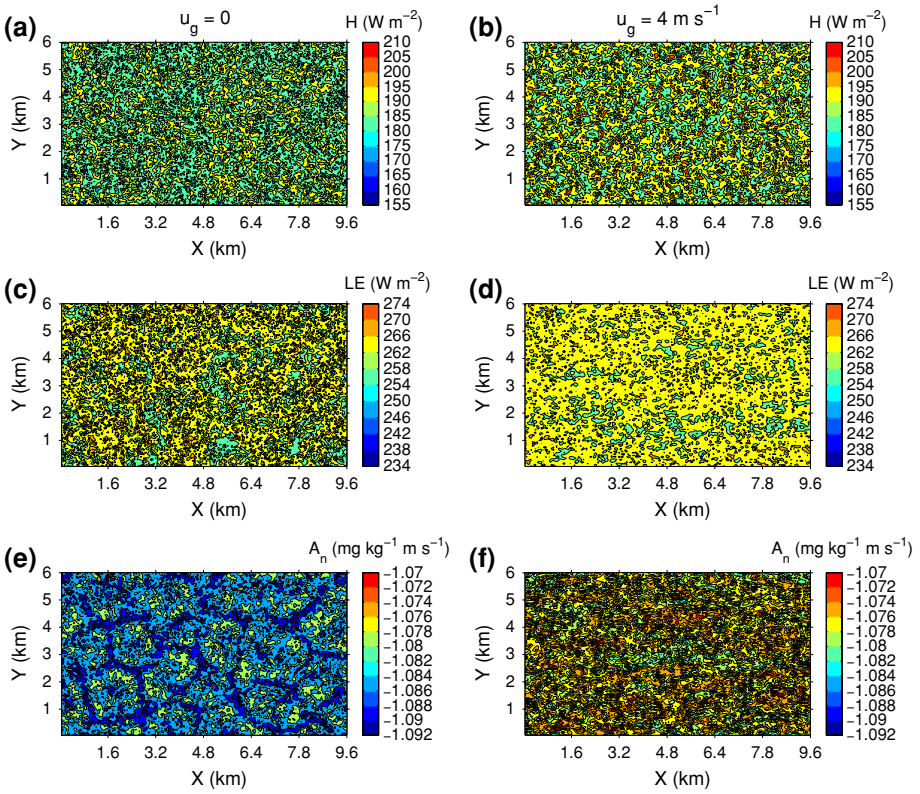

Fig. 8 Hourly-averaged surface fluxes of sensible heat (H, Wm^{-2}, *panels a* and *b*), latent heat (LE : Wm^{-2}, *panels c* and *d*), CO_2 (A_n, $\mathrm{mg\,kg}^{-1}\mathrm{m\,s}^{-1}$, *panels e* and *f*) for the homogeneous case wet ($f_5 = 0.3$) under free ($u_g = 0$, *left side*) and forced convection ($u_g = 4\,\mathrm{m\,s}^{-1}$, *right side*) conditions

mixing ratio (C) at the first level of the LES model. For heterogeneous surface moisture cases, C_r is first calculated for each stripe and then averaged over the whole domain. In the interest of brevity, the data are averaged for each u_g value since differences between homogenous and heterogeneous soil moisture forcing are very small. The surface H shows a strong positive correlation with U and moderate negative correlation with T_a. These correlations become stronger as u_g increases and are consistent with Eq. 2a: at grids with higher wind speeds we expect higher g_a and at grids where T_a is lower we expect the gradient $T_s - T_a$ to be large, both producing a higher H. The surface A_n also exhibits a moderate negative correlation with U. Further analysis reveals that it is T_s that drives the spatial variation in A_n: the correlation between T_s and A_n is almost perfect (0.99). On the other hand, little correlation exists between LE and U, probably because g_a appears in both the numerator and the denominator of Eq. 2b, cancelling much of the wind effect. The main driver of the LE variations appears to be T_a in the surface layer. At grid points with higher T_a, the vapour pressure deficit (VPD) is higher, resulting in a higher LE. Also, indeed, the correlation coefficient between LE and VPD is significant, varying in the range of 0.40 to 0.45 for the simulations presented in Table 1. It is worth noting that LE increases with VPD but only up to the point beyond which stomatal control begins to limit transpiration.

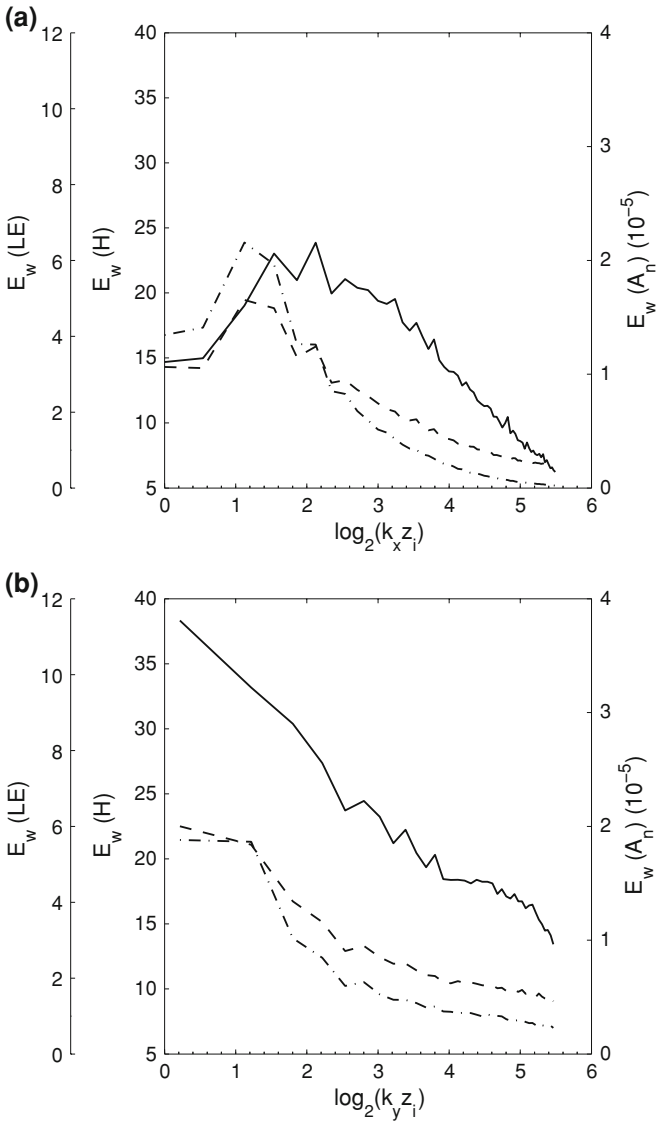

Fig. 9 Energy spectra of surface sensible heat flux (*solid line*), latent heat flux (*dash line*), and CO_2 flux (*dashed dotted line*) along (**a**) the x and (**b**) y direction for homogeneous case B ($f_5 = 0.3$) under $u_g = 4\,\mathrm{m\,s^{-1}}$

Figure 10 shows time series of instantaneous surface fluxes (H, LE, and A_n) at the central point of the simulation domain for the same cases as in Fig. 8. As with the spatial variations, the largest temporal variation is seen in H and the smallest in A_n. These temporal variations decrease as u_g increases. In the free convective limit, H and LE both show large downward spikes corresponding to times when the wind speed is low. For $u_g = 4\,\mathrm{m\,s^{-1}}$, weak ramp structures are visible in H as evidenced by steep rises followed by slow decreases in the time series, but are not clear for LE. In a related study, Su et al. (1996) coupled a photosynthesis model, a leaf stomatal conductance model with a single-leaf energy balance equation, and

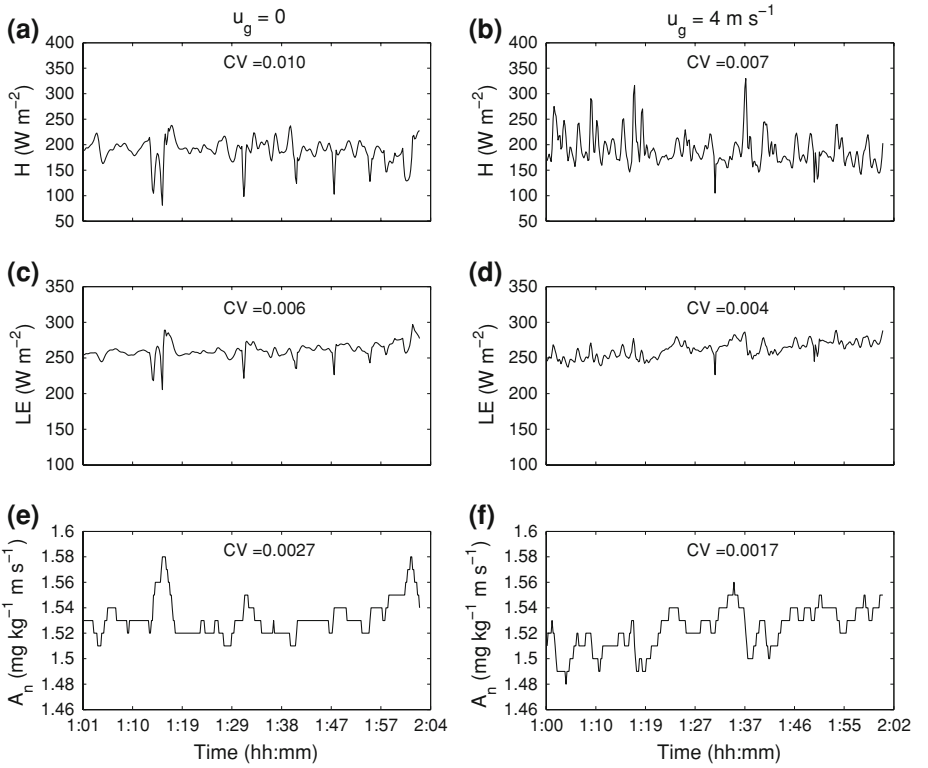

Fig. 10 Time series of instant surface fluxes of sensible heat (H, W m^{-2}, *panels a* and *b*), latent heat (LE, W m^{-2}, *panels c* and *d*), CO_2 (A_n, mg kg^{-1} m s^{-1}, *panels e* and *f*) at the central point of the LES domain for the homogenous wet case (with $f_5 = 0.3$) under free ($u_g = 0$, *left side*) and forced convection ($u_g = 4$ m s^{-1}, *right side*) conditions. Also provided is the coefficient of variation (CV)

found that the TOSs account for most of the intermittency of the eddy-covariance heat flux. Their time series of the subgrid volume-averaged CO_2 assimilation rate exhibits less variation than those of the subgrid volume-averaged sensible and latent heat fluxes.

4.5 Importance of TOS on LSM-Predicted Surface Fluxes

In the three-dimensional (3D) LES-LSM simulations discussed above, the surface fluxes (H, LE, and A_n) are determined locally at each horizontal grid point in direct response to LES-predicted fields that in turn respond to any given heterogeneous surface forcing; therefore, the interaction of the TOS and the dynamic feedback on surface-air exchange is explicitly captured. NWP and climate models are unable to resolve these structures and their impact on the surface fluxes. In this section we address the question: to what extent do NWP and climate models misrepresent surface-atmosphere interactions because of their inability to resolve the flow heterogeneity associated with TOSs?

To answer this question, we used horizontally-averaged surface fluxes from the 3D coupled LES-LSM simulations as a benchmark against which predictions from a version of the LSM attempting to represent the average surface fluxes across the entire LES domain

Table 2 Correlation coefficients for sensible heat (H), latent heat (LE), CO_2 fluxes (A_n) and surface skin temperature (T_s) with wind speed (U), potential temperature (θ), water vapour (q), and CO_2 concentrations (C) at model level 1 for different u_g values

	$u_g\,(\mathrm{m\,s^{-1}})$	U	θ	q	C	T_s
H	0	0.61	−0.27	−0.03	0.11	−0.30
	2	0.67	−0.36	−0.14	0.24	−0.23
	4	0.75	−0.53	−0.34	0.43	−0.22
	6	0.77	−0.62	−0.44	0.48	−0.21
LE	0	−0.11	0.42	−0.05	−0.03	0.54
	2	0.07	0.35	−0.11	0.03	0.50
	4	0.05	0.32	−0.07	0.00	0.67
	6	0.02	0.31	−0.04	0.02	0.77
A_n	0	−0.51	0.66	0.32	−0.41	0.99
	2	−0.42	0.61	0.33	−0.42	0.99
	4	−0.41	0.64	0.38	−0.42	0.99
	6	−0.44	0.64	0.44	−0.41	0.99
T_s	0	−0.51	0.62	0.33	−0.41	–
	2	−0.43	0.56	0.35	−0.43	–
	4	−0.44	0.59	0.39	−0.44	–
	6	−0.46	0.61	0.46	−0.44	–

(e.g., $9.6 \times 6.0\,\mathrm{km}^2$) are evaluated. Initial soil moisture conditions for this separate but identical copy of the LSM code are generated by horizontally averaging soil moisture conditions imposed on the turbulence-resolving 3D coupled LES-LSM. Horizontally- and hourly-averaged atmospheric quantities (T_a, U, q, C) from the lowest atmospheric model level in the 3D coupled LES-LSM system are used to drive the LSM. By horizontally averaging the soil and atmospheric conditions across the entire horizontal LES domain, predictions of H, LE and A_n from this LSM mimic surface fluxes predicted by coarser resolution NWP and climate models. The atmospheric quantities are specified *a priori* and are therefore not permitted to respond to the surface fluxes predicted by the LSM. In what follows, this LSM version will be referred to as the AVG-LSM.

Surface sensible heat, latent heat, and CO_2 flux predictions from the AVG-LSM are compared against horizontally- and time-averaged predictions from the 3D coupled LES-LSM (Table 3). The values in Table 3 represent the percentage difference between, (i) surface fluxes predicted by the AVG-LSM, and (ii) surface fluxes predicted by the 3D coupled LES-LSM

Table 3 Percentage difference (%) of surface sensible heat, latent heat and CO_2 fluxes between 1D parameterization scheme (aggregated values in parenthesis) and the LES-LSM simulations

Cases	H	LE	A_n
A	−3.5	3.3	2.0
B	−4.0	2.1	1.0
C	−8.1 (−4.0)	7.4 (2.8)	8.5 (1.4)
D	−7.8 (−3.8)	7.2 (2.6)	8.2 (1.1)
E	−7.8 (−3.9)	7.6 (2.9)	8.5 (1.4)

Table 4 Domain-averaged sensible ($\langle H \rangle, \mathrm{W\,m^{-2}}$), latent ($\langle LE \rangle, \mathrm{W\,m^{-2}}$) heat fluxes, CO_2 ($\langle A_n \rangle$, $\mathrm{mg\,kg^{-1}\,m\,s^{-1}}$) flux, heat storage term ($\langle S \rangle, \mathrm{W\,m^{-2}}$), and net radiation ($\langle R_n \rangle, \mathrm{W\,m^{-2}}$) for homogeneous case ($f_5 = 0.2$) and the three surface heterogeneous patterns ($a = 1/2, 1/4, 1/8$)

Surface pattern	$\langle H \rangle$	$\langle LE \rangle$	$\langle S \rangle$	$\langle A_n \rangle$	$\langle R_n \rangle$
Homogeneous	209.3	237.9	0.6	1.062	447.8
$a = 1/2$	215.7	230.9	−0.5	0.996	447.6
$a = 1/4$	215.9	230.7	−0.6	0.996	447.6
$a = 1/8$	218.7	227.1	−1.0	0.992	446.8

system that have been horizontally and time averaged. The data in Table 3 are averages over each of the four simulations per case (i.e., across variations in geostrophic wind).

For the two cases with homogeneous soil moisture (A and B), the AVG-LSM underestimates the surface sensible heat flux by about 4%, overestimates the surface latent heat flux by 2–3%, and overestimates surface CO_2 flux by 1–2%. Therefore, in situations where the only flow heterogeneity in the system is that generated by the TOS, a 1D representation captures the surface exchange reasonably well.

Soil moisture heterogeneity magnifies the surface-flux bias predicted by the AVG-LSM. Further examination of the calculations reveals that the AVG-LSM underpredicts the aerodynamic conductance, g_a, leading to an underestimation of H (see Eq. 2a). On the other hand, the AVG-LSM overpredicts both the canopy conductance to water vapour and to CO_2, which leads to an overestimation of water vapour and CO_2 fluxes in the climate models (see Eq. 2a, b). However, these biases remain within 10%.

To separate the effect of surface parameter nonlinearity from that of the ABL flow heterogeneity for the cases with heterogeneous surface forcing (C to E), we performed another group of calculations. In this group of calculations, we used the horizontally- and time-averaged atmospheric conditions from each case (C to E) to force the AVG-LSM but performed this calculation twice (once with soil moisture conditions $f_5 = 0.1$ and again with $f_5 = 0.3$) and then subsequently averaged the predicted fluxes from each. These calculations resemble aggregated schemes such as those discussed in Doran et al. (1998) and are meant to remove the effects of parameter nonlinearities. Any difference between the aggregated AVG-LSM prediction and the coupled LES-LSM simulation represents the influence from ABL flow heterogeneity. The results, presented in parentheses in Table 3, suggest that for sensible heat flux, ABL flow heterogeneity is equally important as parameter nonlinearity, and that flow heterogeneity is more important for water vapour and CO_2 fluxes than is parameter nonlinearity. We also note a consistent bias associated with ABL flow heterogeneity across all heterogeneous simulations (C to E).

Finally, the coupled LES-LSM results show that the surface moisture heterogeneity modifies the energy balance partitioning. As an example, Table 4 compares the domain-averaged surface fluxes for the three heterogeneous cases with those under homogeneous moisture forcing ($f_5 = 0.2$) at $u_g = 2\,\mathrm{m\,s^{-1}}$. The surface latent heat flux (LE) decreases while the sensible heat flux (H) increases as the surface heterogeneity scale decreases, which is consistent with the results of Courault et al. (2007). The ratio of H to LE increases from 0.88 to 0.96 as the patch number increases for the cases with $u_g = 2\,\mathrm{m\,s^{-1}}$; a similar relationship exists for other wind speeds (results not shown). Although these changes are relatively small in comparison to the uncertainty inherit in atmospheric models, they represent systematic biases associated with the 1D LSM applications.

5 Summary and Conclusions

A coupled LES-LSM model has been used to quantify the impact of surface and ABL flow heterogeneities on the vegetation-atmosphere exchange of heat, water vapour and CO_2. We show that the eddy diffusivity for CO_2 is different from those for heat and water vapour in the surface layer, with the inequality attributed to local advection induced by surface moisture heterogeneity and top-down diffusion promoted by entrainment at the top of ABL. The surface heterogeneity imposes different influences on the spatial structures of the three scalar fields. The CO_2 turbulence-organised structures bear more resemblance to those of water vapour than those of the potential temperature. The surface fluxes when coupled with the flow aloft show large spatial variabilities even with homogeneous surface moisture and solar radiation forcing. The peak wavelengths of the surface flux variations are smaller than those of vertical velocity, temperature and other scalars in the middle regions of the boundary layer. Among the three scalars investigated, the surface sensible heat flux shows the highest spatial and temporal variations and the CO_2 flux the lowest.

The 1D LSM scheme as adopted in NWP and climate models ignores ABL flow heterogeneity and parameter nonlinearity that occur at scales smaller than the grid size of these models. Despite this, the 1D LSM surface-flux predictions show very good performance as compared to the LES-LSM results. The 1D LSM prediction biases of the three surface fluxes are less than 4% for homogeneous surface forcing. Surface heterogeneity causes slightly higher prediction errors (up to 9%).

Acknowledgements This research was supported by the U.S. Department of Energy's Office of Science (BER) through the Northeastern Regional Center of the National Institute for Climatic Change Research. This research used resources of the National Energy Research Scientific Computing Center, which is supported by the Office of Science of the U.S. Department of Energy.

References

Avissar R, Schmidt T (1998) An evaluation of the scale at which ground-surface heat flux patchiness affects the convective boundary layer using large-eddy simulations. J Atmos Sci 55:2666–2689. doi:10.1175/1520-0469(1998)055<2666:AEOTSA>2.0.CO;2

Beljaars ACM, Holtslag AAM (1991) Flux parameterization over land surfaces for atmospheric models. J Appl Meteorol 30:327–341. doi:10.1175/1520-0450(1991)030<0327:FPOLSF>2.0.CO;2

Courault D, Drobinski P, Brunet Y, Lacarrere P, Talbot C (2007) Impacts of surface heterogeneity on a buoyancy-driven convective boundary layer in light winds. Boundary-Layer Meteorol 124:383–403. doi:10.1007/s10546-007-9172-y

Deardorff JW (1979) Prediction of convective mixed-layer entrainment for realistic capping inversion structure. J Atmos Sci 36:424–436. doi:10.1175/1520-0469(1979)036<0424:POCMLE>2.0.CO;2

Denmead OT, Bradley EF (1985) Flux-gradient relationships in a forest canopy. In: Hutchison BS, Hicksedes BB (eds) The forest-atmosphere interaction. D. Reidel Publishing Co, Dordrecht, pp 421–442

Doran JC, Hubbe JM, Liljegren JC, Shaw WJ (1998) A technique for determining the spatial and temporal distribution of surface fluxes of heat and moisture over the Southern Great Plains Cloud and Radiation Testbed. J Geophys Res 103:6109–6121. doi:10.1029/97JD03427

Dyer AJ (1974) A review of flux-profile relationships. Boundary-Layer Meteorol 7:363–372. doi:10.1007/BF00240838

Ek MB, Mitchell KE, Lin L, Rogers E, Grunmann P, Koren V, Gayno G, Tarpley JD (2003) Implementation of NOAH land surface model advances in the National Center for Environmental Prediction operational mesoscale Eta model. J Geophys Res 102:28987–28996

Gao W, Shaw RH, Paw UKT (1989) Observation of organized structure in turbulent flow within and above a forest canopy. Boundary-Layer Meteorol 47:349–377. doi:10.1007/BF00122339

Garratt JR (1992) The atmospheric boundary layer. Cambridge University Press, Cambridge, U.K., 316 pp

Hadfield MG, Cotton WR, Pielke RA (1991) Large-eddy simulations of thermally forced circulations in the convective boundary layer. Part I: a small-scale circulation with zero wind. Boundary-Layer Meteorol 57:79–114. doi:10.1007/BF00119714

Hadfield MG, Cotton WR, Pielke RA (1992) Large-eddy simulations of thermally forced circulations in the convective boundary layer. Part II: the effect of changes in wavelength and wind speed. Boundary-Layer Meteorol 58:307–327. doi:10.1007/BF00120235

Huang JP, Lee X, Patton EG (2008) A modelling study of flux imbalance and the influence of entrainment in the convective boundary layer. Boundary-Layer Meteorol 127:273–292. doi:10.1007/s10546-007-9254-x

Idso SB (1981) A set of equations for full spectrum and 8- to 14- µm and 10.5- to 12.5- µm thermal radiation from cloudless skies. Water Resour Res 17:295–304. doi:10.1029/WR017i002p00295

Jarvis PG (1976) The interpretation of the variations in leaf water potential and stomatal conductance found in canopies in the field. Phil Trans Roy Soc Lond 273B:593–610. doi:10.1098/rstb.1976.0035

Jonker HJJ, Duynkerke PG, Cuijpers JWM (1999) Mesoscale fluctuations in scalars generated by boundary convection. J Atmos Sci 56:801–808. doi:10.1175/1520-0469(1999)056<0801:MFISGB>2.0.CO;2

Kanda M, Inagaki A, Letzel MO, Raasch S, Watanabe T (2004a) LES study of the energy imbalance problem with eddy covariance fluxes. Boundary-Layer Meteorol 110:381–404. doi:10.1023/B:BOUN.0000007225.45548.7a

Kanda M, Moriwaki R, Kasamatsu F (2004b) Large-eddy simulation of turbulent organized structures within and above explicitly resolved cube arrays. Boundary-Layer Meteorol 112:343–368. doi:10.1023/B:BOUN.0000027909.40439.7c

Lee X, Yu Q, Sun X, Liu J, Min Q, Liu Y, Zhang X (2004) Micrometeorological fluxes under the influence of regional and local advection: a revisit. Agric For Meteorol 122:111–124. doi:10.1016/j.agrformet.2003.02.001

Mahrt L (1998) Flux sampling errors for aircraft and towers. J Atmos Ocean Technol 15:416–429. doi:10.1175/1520-0426(1998)015<0416:FSEFAA>2.0.CO;2

McNaughton KG, Laubach J (1998) Unsteadiness as a cause of non-equality of eddy diffusivities for heat and vapour at the base of an advective inversion. Boundary-Layer Meteorol 88:479–504. doi:10.1023/A:1001573521304

Moeng CH (1984) A large-eddy simulation model for the study of planetary boundary-layer turbulence. J Atmos Sci 41:2052–2062. doi:10.1175/1520-0469(1984)041<2052:ALESMF>2.0.CO;2

Patton EG, Sullivan PP, Moeng CH (2005) The influence of idealized heterologeneity on wet and dry planetary boundary layers coupled to the land surface. J Atmos Sci 62:2078–2097. doi:10.1175/JAS3465.1

Paw UKT, Brunet Y, Collineau S, Shaw RH, Maitani T, Qin J, Hipps L (1992) On coherent structures in turbulence above and within agricultural plant canopies. Agric For Meteorol 61:55–68. doi:10.1016/0168-1923(92)90025-Y

Ronda RJ, Bruin HARD, Holtslag AAM (2001) Representation of the canopy conductance in modelling the surface energy budget for low vegetation. J Appl Meteorol 40:1431–1444. doi:10.1175/1520-0450(2001)040<1431:ROTCCI>2.0.CO;2

Shen SH, Leclerc MY (1995) How large must surface inhomogeneities be before they influence the convective boundary layer structure? A case study. Q J Roy Meteorol Soc 121:1209–1228. doi:10.1002/qj.49712152603

Steinfeld G, Letzel MO, Raasch S, Kanda M, Inagaki A (2007) Spatial representativeness of single tower measurements and the imbalance problem with eddy-covariance fluxes: results of a large-eddy simulation study. Boundary-Layer Meteorol 123:77–98. doi:10.1007/s10546-006-9133-x

Su HB, Paw UKT, Shaw RH (1996) Development of a coupled leaf and canopy model for the simulations of plant-atmosphere interactions. J Appl Meteorol 35:722–748. doi:10.1175/1520-0450(1996)035<0733:DOACLA>2.0.CO;2

Sullivan PP, McWilliams JC, Moeng CH (1994) A subgrid-scale model for large-eddy simulation of planetary boundary-layer flows. Boundary-Layer Meteorol 71:247–276. doi:10.1007/BF00713741

Sullivan PP, McWilliams JC, Moeng CH (1996) A grid nesting method for large-eddy simulation of planetary boundary-layer flows. Boundary-Layer Meteorol 80:167–202. doi:10.1007/BF00119016